Analyst

Near-field infrared nanospectroscopy and super-resolution fluorescence microscopy enable complementary nanoscale analyses of lymphocyte nuclei

Journal:	*Analyst*
Manuscript ID	AN-ART-07-2018-001341.R1
Article Type:	Paper
Date Submitted by the Author:	03-Sep-2018

Complete List of Authors:	Ajaezi, Godwin; University of Manitoba Faculty of Science, Chemistry; University of Manitoba Faculty of Engineering, Biomedical Engineering Program Eisele, Max; Neaspec GmbH Contu, Fabio; University of Manitoba College of Medicine, Physiology and Pathophysiology; University of Cagliari, Department of Biomedical Sciences, Unit of Biology and genetics Lal, Sadhana; Genomic Centre for Cancer Research and Diagnosis; Research Institute of Oncology and Hematology, CancerCare, Cell Biology Rangel-Pozzo, Aline; University of Manitoba College of Medicine, Physiology and Pathophysiology Mai, Sabine; University of Manitoba College of Medicine, Physiology and Pathophysiology; Genomic Centre for Cancer research and Diagnosis; Research Institute of Oncology and Hematology, CancerCare, Cell Biology Gough, Kathleen; University of Manitoba Faculty of Science, Chemistry; University of Manitoba Faculty of Engineering, Biomedical Engineering Program

Journal Name

ARTICLE

Near-field infrared nanospectroscopy and super-resolution fluorescence microscopy enable complementary nanoscale analyses of lymphocyte nuclei

Received 00th January 20xx,
Accepted 00th January 20xx

DOI: 10.1039/x0xx00000x

www.rsc.org/

Godwin C. Ajaezi [a,b], Max Eisele[c], Fabio Contu [d,e], Sadhana Lal [f,g], Aline Rangel-Pozzo [d], Sabine Mai [d,f,g] and Kathleen M. Gough *[a,b]

Recent super-resolution fluorescence microscopy (3D-Structured Illumination Microscopy, 3D-SIM) studies have revealed significantly altered nuclear organization between normal lymphocyte nuclei and those of classical Hodgkin's Lymphoma. Similar changes have been found in Multiple Myeloma (MM) nuclei, as well as in a premalignant condition, Monoclonal Gammopathy of Unknown Significance (MGUS). Using 3D-SIM, an increase in DNA-poor and DNA-free voids was evident in reconstructed 3D-SIM images of diseased nuclei at 40 nm pixel resolution *(x,y*: 40nm, *z*: 80nm). At best, far-field FTIR imaging yields spatially resolved images at ~500 nm spatial resolution; however, near-field infrared imaging breaks the diffraction limit at a scale comparable to that of 3D-SIM, providing details on the order of 30 nm spatial resolution. We report here the first near-field IR imaging of lymphocyte nuclei, and far-field IR imaging results of whole lymphocytes and nuclei from normal human blood. Cells and nuclei were mounted on infrared-compatible substrates, including CaF_2, undoped silicon wafers, and gold-coated silicon wafers. Thermal source far-field FTIR images were obtained with an Agilent-Cary 620 microscope, 15x objective, 0.62 NA and 64x64 array Focal Plane Array detector (University of Manitoba), or with a similar microscope equipped with both 15x and 25x (0.81 NA) objectives, 128x128 FPA and either thermal source or synchrotron source (single beam) infrared light at the Advanced Light Source (ALS), LBNL, Berkeley CA. Near-field IR spectra were acquired at the ALS, on the in-house SINS equipment, as well as with a Neaspec system, both illuminated with synchrotron light. Finally, some near-field IR spectra and images were acquired at Neaspec GmbH, Germany. Far-field IR spectra of normal cells and nuclei showed the characteristic bands of DNA and proteins. Near-field IR spectra of nuclei showed variations in bands assigned to protein and nucleic acids including single and double-stranded DNA. Near-field IR images of nuclei enabled visualization of protein and DNA distribution in spatially-resolved chromosome territories and nuclear pores.

.

Introduction

Conventional and super resolution fluorescence (SRF) imaging are important tools in the analysis of normal and diseased cells. With the advent of SRF imaging, the architecture of the nucleus, in particular that of nuclear DNA organization and of chromosome territories (CTs) in the interphase nucleus, were studied for the first time at a spatial resolution of 40 nm.[1-5] An increase in DNA-free or DNA-poor spaces was identified in the nuclei of classical Hodgkin's Lymphoma, both in the mononucleated Hodgkin (H) cells and in the bi- and multi-nucleated Reed-Sternberg (RS) cells when compared to normal (NL) lymphocytes. Similar DNA-poor spaces have since been identified in multiple myeloma (MM) cells and their precursor cells: monoclonal gammopathy of undetermined significance (MGUS),[3] as well as in the nuclei of buccal cells in Alzheimer's Disease.[5] The biological significance of these spaces may relate to the state/stage and aggressiveness of the disease. For example, MGUS has fewer DNA-poor spaces than MM and both have more than control lymphocytes.[3] In MM, the organization of CTs was examined comparatively using conventional 3D microscopy (with the Abbe limit of 200nm) and 3D-SIM. Shared and distinct CTs were identified.[4] The formation of DNA-poor spaces may be a general step in the development of many diseases, but the detailed changes may be disease-specific. The analysis of these DNA-poor and DNA-free regions is limited by the lack of tools for detecting their biochemical composition at a nm length scale.

Infrared spectroscopy has been a mainstay for chemical analysis for many decades[6] but the rich chemical information delivered by this technique has been restricted to diffraction-limited spectrochemical images, on the order of a micron, at best. Near-field infrared techniques have recently brought the

[a] Chemistry, University of Manitoba, Winnipeg, MB, Canada.
[b] Biomedical Engineering Program, University of Manitoba, Winnipeg, MB, Canada.
[c] Neaspec GmbH, Bunsenstrasse 5, 82512 Martinsried, Germany
[d] Physiology and Pathophysiology, University of Manitoba, Winnipeg, MB, Canada.
[e] Department of Biomedical Sciences, Unit of Biology and Genetics, University of Cagliari, Italy;
[f] Genomic Centre for Cancer Research and Diagnosis, Winnipeg, MB, Canada.
[g] Cell Biology, Research Institute of Oncology and Hematology, CancerCare Manitoba, Winnipeg, MB, Canada.

Electronic Supplementary Information (ESI) available: [details of any supplementary information available should be included here]. See DOI: 10.1039/x0xx00000x

spatial resolution capability of this technique into the same length scale as SRF.[7-12]

We present here the first scattering Scanning Nearfield Optical Microscopy (sSNOM) infrared study of NL nuclei as the first step in a larger study of normal and diseased nuclei. Sample preparation protocols have been devised in order to obtain bare nuclei that are thin enough for true nanoscale analysis.

Experimental

Materials

Peripheral blood was obtained from healthy donors who signed informed consent according to the institutional approval of University of Manitoba's Health Research Ethics Board Protocol (#HS14085(H2011:336)).

Lymphocyte preparation for SRF. Peripheral blood from volunteer donors was overlaid on Ficoll (GE Healthcare, Uppsala, Sweden) and centrifuged at 200g for 30 minutes to isolate the control lymphocytes. The buffy coat was removed and washed in PBS; cells were re-suspended in a lower volume of PBS and spread on poly-L-lysine coated slides (Sigma-Aldrich, St. Louis, MO, USA) for immunohistochemistry staining.

The Hodgkin's derived cell line HDLM-2 was grown in RPMI-1640 medium, supplemented with 20% fetal bovine serum (FBS), 1% L-glutamine, and 1% penicillin–streptomycin (Invitrogen/Gibco, Burlington, Canada). Cells were incubated at 37°C with 5% CO_2 in a humidified atmosphere, washed with PBS and gently placed onto poly-L-lysine coated slides.

Immunohistochemistry for the upstream binding factor (UBF) in NL and HL-derived cell line HDLM-2 was performed using primary UBF antibody (ab) (rabbit polyclonal, H-300, sc-9131, Santa Cruz, Dallas, USA) and secondary Goat anti-rabbit Alexa 488 ab (Molecular Probes, Eugene, USA) with a dilution of 1:60 and 1:500 respectively in 4% BSA/4×SSC blocking solution. Cells underwent fixation in 3.7% formaldehyde/1×PBS and permeabilization with 0.1% Triton X-100, followed by three 1X PBS washes, with shaking at room temperature (RT). Incubation with primary ab was performed for 45 minutes at RT and followed by three 1X PBS washes, with shaking at RT. Incubation with secondary ab was performed for 30 minutes at RT and followed by three 1X PBS washes with shaking at RT. Cells were counterstained with 50µl of 1 µg/mL of DAPI (4',6-diamidino-2-phenylindole) for 5 min at RT. A drop of Vectashield (Vector Labs, Burlingame, CA) was used to embed the slides to prevent photo-bleaching.

Lymphocyte and nuclei preparation for infrared analyses. Ten mL of EDTA whole peripheral blood was drawn from volunteer donors, diluted with 2 mL normal saline (0.9%, NS). Cells were separated in Ficoll as above, at 210g, 30 min. The buffy coat cells were resuspended in 5 mL NS and washed (210g, 5 min); the pellet was resuspended in 5 mL RBC lysis buffer to eliminate residual red blood cells (210g, 5 min). The cell pellet was washed 6x by suspension in 8 mL NS followed by centrifugation (210g, 5 min). The final cell pellet was resuspended in 1mL NS. For initial trials, 2µL of the cell suspension was dropped onto an IR substrate and air-dried. In later experiments, a 60µL aliquot of the cell suspension was spun onto the substrate using a cytofuge (Elliot-Shandon Cytospin, model 00-20) at 200g, 5 min.

To obtain the bare lymphocyte nuclei, a washed cell pellet was treated with NP-40 in modified RSB buffer (10mM Tris, pH 7.2, 10mM NaCl, 3mM $MgCl_2$; 1:2500). The resuspended cells were homogenized using a tissue homogenizer (DWK Life Sciences Kimble, Kontes™ Dounce) and centrifuged (180g, 5 min). After resuspension in 1mL NS, a 70µl aliquot of stripped nuclei was cytofuged onto an IR substrate (200g, 5 min).

Substrates for infrared data collection. BaF_2 and CaF_2 windows were used for far-field transmission IR imaging. Gold-coated silicon (AuSi) wafers prepared in-house and undoped, single-side polished Si wafers (University Wafer Inc., USA) were cut into ~1 cm squares for far-field transflection and near-field IR experiments. After cells or nuclei were mounted, wafers were air dried and stored in sealed plastic cases, in the dark, at RT, until data acquisition, normally within a few days.

Methods

SRF microscopy. All images were captured with a Zeiss Elyra PS1 SIM equipped with a Plan-Apochromat 63x/1.40 oil immersion objective and an Andor EM-CCD iXon 885 camera and a 1.6x tube lens, at RT. The DAPI channel was obtained with 405nm laser excitation, 28µm diffraction grating; the Alexa488 of the UBF was obtained using the FITC channel with 488nm laser excitation, 28µm diffraction grating. Images of the z-stacks were acquired using 3 grid orientations and 5 phases. The step size between z-planes, Δz, was set at 91 nm. The 3D-SIM and widefield images were reconstructed with ZEN 2012 black edition (Carl Zeiss, Jena, Germany) with the standard settings except for the noise filter, which was set to -3.0. The clipping function was turned off to prevent loss of image information. Pixel size (Δx, Δy) was 79nm in the raw images and 40nm in the reconstructed images.

Far field Fourier transform infrared spectroscopy. Some far-field FTIR images were acquired with an Agilent Cary 670 interferometer and 620 infrared microscope equipped with a 64 x 64 FPA, thermal light source, 15x (0.62 NA) objective, with additional optional optics in front of the FPA, to yield a maximum spatial resolution of 1.1 µm (Spectromicroscopy Imaging Laboratory, University of Manitoba). Other far field data were acquired on a similar Agilent Cary 670/620 microscope at ALS. In addition to the 15x objective, this instrument had a 25x (0.81 NA) objective, and 128 x 128 FPA detector; high magnification optics gave maximum magnification of nominal 0.7 µm pixel edge. Thermal source (globar) and synchrotron source illumination were used. Data were collected in transmission and transflection mode, depending on substrate. Spectra were typically collected as a sum of 128 sample scans, ratioed against 512 background scans, at 4cm^{-1} spectral resolution.

Near-field infrared spectroscopy at ALS. Near-field FTIR spectra were collected with the in-house designed[10] Synchrotron Infrared NanoSpectroscopy instrument (aka SINS) on B.L. 5.4 at the Advanced Light Source, Berkeley, California. The 1 cm square AuSi sample wafer was firmly taped to a block and mounted onto the magnetic stage. The position was manually adjusted to put the target cell within the accessible field of view. A modified AFM (Innova, Bruker) illuminated with synchrotron light, and a modified commercial rapid-scan FTIR spectrometer (Nicolet 6700, Thermo-Scientific), coupled with an asymmetric Michaelson interferometer enabled acquisition of AFM images and SINS spectra.[10] For each background and sample spectrum, 600 scans were co-added at 8cm^{-1} spectral resolution. A fresh background spectrum was taken every 30 to 60 minutes. The second order amplitude and phase backscattered light were post-processed in a Fast Fourier Transform analysis package (Nanospectroscopy Data Analysis V.1) developed in-house for BL 5.4 at ALS, to give near-field infrared spectra as absorbance.

Some cells measured at BL 5.4 were then examined with a Neaspec NanoFTIR illuminated with synchrotion radiation at BL 2.4, ALS. The second order amplitude and phase back scattered light were recorded by co-addition of 600 scans for both background and sample. Post-processing of data was carried with neaPLOTTER software (Neaspec, Germany) to obtain absorption spectra.

Near-field infrared spectroscopy at Neaspec. Near-field IR spectra and images of cells and nuclei on AuSi, including cells imaged at BL 5.4, ALS and cells on undoped Si wafers, were obtained at Neaspec (Neaspec GmbH, Germany). Mid-IR wavelengths for the latter were supplied by either a broadband mid-IR nano-FTIR illumination unit or at selected single wavelengths from one of a set of Quantum Cascade Lasers (QCLs). For single frequency contrast imaging, the QCL was set to match a component band maximum, with the exception of an observed peak at 965 cm^{-1}. An instability in the Neaspec QCL required that it be set to 956 cm^{-1}; given the band width, this was adequate to highlight the DNA distribution. Results were processed as above.

Results and Discussion

Our motivation for this work is to establish a robust methodology for near-field infrared imaging of nuclei, in order to compare normal and diseased cells. As has been shown through SRF, normal nuclei and those of diseased nuclei display distinctly different nuclear organization. This was established using quantitative imaging of telomeres, centromeres, chromosomes and their orientation.[1-5, 13-19] These data indicate that the nuclear organization is significantly altered in diseased cells and may serve as a structural biomarker for disease states and progression.[20-22]

SRF of NL and HL nuclei

Superresolution fluorescence images show the nuclear organization of DNA of a normal interphase nucleus, and disturbed architecture in H and RS nuclei (Fig. 1). The distinct organization of the genome and the presence vs. absence of DNA-poor spaces in the form of increased interchromatin and circular DNA-poor spaces in the malignant cells are depicted in Fig. 1A (normal lymphocyte) and 1B-D (Hodgkin's lymphomoa), respectively. The nucleolar phosphoprotein UBF is located in the nucleolus; however, DNA-poor spaces of H and RS cells do not contain UBF.[1] Green-filled arrow heads indicate nucleoli containing UBF; black-filled arrowheads indicate DNA-poor spaces lacking UBF. As expected, the normal nucleus (Fig. 1A) is much smaller than the H and RS.[1] The nucleoli are also much smaller; here, only one small nucleolus is visible. The large H and RS cells contain multiple large nucleoli and DNA-poor circular regions; only the more prominent examples are denoted (Fig. 1 B-D). Videos of the concatenated z-stack images show normal nucleoli with UBF and DNA-poor regions throughout the full volume of NL, H and RS nuclei (ESI, video 1 NL, video 2 H, video 3 RS-binucleate and video 4 RS-tetranucleate). A similar H cell stained with nucleolin instead of UBF provides an alternative visualization of these DNA-poor regions. (ESI Fig. 1, video 5).

Fig. 1 Single z-plane widefield images of nuclei stained with DAPI SIM (grayscale) and UBF (green) from (**A**) normal isolated peripheral-blood lymphocyte (NL), (**B**) Hodgkin (H) cell, (**C**) bi-nuclear and (**D**) tetra-nuclear Reed-Sternberg (RS) cells from the cHL derived cell line HDLM-2. Green-filled arrowheads indicate nucleoli containing UBF; black-filled arrowheads indicate DNA-poor spaces not containing UBF.

AFM of whole cells and nuclei for near-field IR

Initial preparations of whole lymphocytes were found to be inadequate for NFIR spectroscopy. In early tests, 2 to 4 µL aliquots of resuspended lymphocytes were deposited on AuSi wafers and air-dried (Fig. 2A). AFM measurements showed that these cells beaded up on the surface and were at least 2µm high; they proved to be too thick for good NFIR. Not only was the signal weak, but lensing of the synchrotron illumination created spectral artefacts (data not shown). Subsequently, suspensions of whole cells were cytofuged onto the substrate, yielding a maximum height of about 1 µm for deposited whole cells (Fig. 2 B). Synchrotron near-field spectra (SINS) could be obtained from points around the edges, but the signal was still poor and dominated by cytoplasm (data not shown). Finally, stripped nuclei were prepared and cytofuged onto AuSi (Fig. 2C). Relative height profiles for each preparation are shown in Fig. 2D. The cytofuged stripped nuclei were ideal for NFIR measurements, particularly in thinner regions where height dropped to ~30 nm.

Fig. 2 AFM topographic images of (**A**) whole NL from droplet preparation, (**B**) whole NL prepared by cyto-centrifugation of cell suspension, (**C**) stripped NL nucleus cytofuged onto AuSi IR substrate, and (**D**) corresponding AFM profiles of the whole lymphocytes and nucleus.

Far field FTIR spectra

Far field FTIR (FFIR) spectrochemical FPA images of whole lymphocytes and nuclei on AuSI wafers were taken on cells and nuclei prepared for near-field IR. Correlated spectra for nuclei on AuSi wafers were not feasible (ESI, Fig. 2) as the well-known Electric Field Standing Wave effect was significantly pronounced for these thin targets imaged in transflection mode off AuSi wafers.[23,24] Nuclei prepared by cytofuging onto 1mm thick CaF_2 windows offered greater opportunity for comparison but the samples were too thin to give adequate signal except when multiple nuclei were overlaid (ESI, Fig. 3), and they could not be imaged with NFIR. The ~300nm thick individual nuclei were identifiable by the broad OH-NH stretch band, but little detail could be discerned in the 1800-900 cm^{-1} region. However, if it is possible to define differences between normal and diseased nuclei with NFIR, we can envision the practical application of FFIR using a more concentrated sample preparation, with classification guided by NFIR analyses.

NFIR of nuclei

Near-field IR spectra of nuclei were obtained in one of three ways: (1) illumination of AFM tip with synchrotron source light at BL 5.4 (SINS), (2) similar data collection but with Neaspec instrument at BL 2.4, both at the ALS; and (3) with mid-IR laser sources, Neaspec GmbH**,** Germany. Finally, single wavelength images were obtained with mid-IR laser sources, Neaspec GmbH**,** Germany.

Spectra and images from Neaspec, GmbH. Point spectra and single wavelength images from a stripped NL nucleus obtained at Neaspec, GmbH, are shown in Fig. 3.

Fig. 3 AFM topography and Near-field IR of stripped NL nucleus cytofuged onto AuSi wafer. (**A**) AFM topography shown in grey scale; (**B**) false-colour image showing total integrated broad band infrared absorption; red circle shows location for background spectrum; (**C**) region in B enlarged for clarity to show locations for two spectral acquisitions. (**D**) Corresponding near-field IR spectra recorded with mid-IR lasers, at positions 1 and 2.

Images revealed physically distinct structures within the nucleus (Fig. 3). From the topographic scan, the stripped nucleus exhibited regions with maximum height of about 1.7µm (Fig. 3A), corresponding to regions with the densest infrared absorbance (Fig. 3B). The thickness at the periphery of the nucleus was far less than 1µm; the appearance and density of thinner regions at the edge suggested that they corresponded to nuclear pores. The thicker, denser regions have the appearance of chromosome territories (CTs), which would be rich in protein and DNA.

In general, thinner locations were found to be the best locations for the collection of strong, clear infrared spectra (Fig. 3C), as can be seen in full spectra recorded at two positions: the denser region, position 1, AFM height 30 nm, and Position 2, AFM height 120nm (Fig. 3D). There are numerous compilations of nucleic acid infrared spectra and conformational marker bands for nucleic acids vary with pH, salt concentrations and hydration; the sharp strong bands seen in this sSNOM NFIR spectrum represent dehydrated nucleic acids in saline. Observed bands and likely assignments proposed here are based on a recent review of extensive studies of DNA-forms, Table 1.[25]

The sample height at position 1 was only 30nm; the signal strength was greater and the spectrum showed dramatically clear DNA signatures corresponding to single (1116 cm^{-1}) and double (1710 cm^{-1}) stranded DNA (Table 1). Both components can be expected in nuclear pores regions, supporting the probable assignment as nuclear pore.

At position 2, AFM height 120nm, the spectrum was dominated by Amide I and II bands at 1655 and 1545 cm^{-1}, along with weaker bands typical of CH deformations (lipids, protein side chains) and phosphates at 1465, 1400 and 1235 cm^{-1}. None of the characteristic nucleic acid bands were evident. In spite of the dense DNA present, the interphase CT is rich in proteins, so the spectrum can be assumed to be from CT. We note that he near-field intensity response was relatively low at position 2, probably owing to the thickness of >100nm (*vide infra*).
A dip at 1265 cm^{-1}, marked with an asterisk (*) appears in most near-field IR spectra and is due to tip contamination with PDMS[26] from the original packaging. That signal is enhanced when the contaminated bare tip is close to clean gold, i. e., when the background spectrum is being acquired; hence, the final appearance in the processed sample spectra is a negative peak.

Single wavelength images from AuSi wafer. The spatial distributions of three prominent bands observed in the two point spectra were imaged under single wavelength illumination (DNA-phosphates at 956 cm^{-1}, protein Amide II at 1545 cm^{-1}, and DNA at 1710 cm^{-1}), relative to response at a point far from the nucleus, bare gold. At 1800 cm^{-1}. The results are shown in Fig. 4.

Fig. 4. NFIR sSNOM single wavelength images of nucleus region from Fig. 3. Top row shows (**A**) AFM topography, (**B**) total integrated IR absorbance and (**C**) 2nd order phase shift under 1800 cm^{-1} illumination. Middle row (**D**-**F**) shows 2nd order phase shifts at given wavelengths; bottom row (**G**-**I**) shows same phase shifts corrected for thickness.

The nuclear pores and dense chromatin regions are identifiable through the topography from the AFM (Fig. 4A) and the total integrated absorbance (Fig. 4B). The phase shift contains the majority of the near-field IR absorbance signal.[7-12] A considerable phase shift is recorded in what should be a non-absorbing wavelength: 1800 cm^{-1}, across the field of view (Fig. 4C). The magnitude of the phase shift diminishes as sample thickness decreases below 50 nm, probably owing to coupling between the gold-coated AFM tip and the gold coated substrate. The magnitude of the raw second order phase shift responses at 956 cm^{-1} (DNA, ribose), 1545 cm^{-1} (Amide II) and 1712 cm^{-1} (DNA) would be affected by this shift (Fig. 4, D-F). This background distortion was subtracted (Fig. 4, G-I) to allow proper visualization of the protein and DNA distributions. The thicker regions, ascribed to interphase chromatin region, are

seen to be rich in protein, while the nuclear pores contain the greatest DNA signals.

Single wavelength images of nucleus on undoped Si wafer. An undoped polished Si wafer was used as a substrate for stripped nuclei to evaluate the suspected tip-substrate coupling on the AuSi wafers described above. Undoped wafers (>10,000 Ohm-cm resistance) were chosen over the more common doped silicon to avoid accidentally hitting a plasma frequency directly in the spectral range to be probed, as this would result in significant confounding absorption profiles. Spectra and single wavelength phase shift images acquired on the Neaspec instrument (Neaspec GmbH, Germany) are shown in Fig. 5.

Fig. 5 Spectra and single wavelength 2nd order phase shift images of a NL nucleus on undoped Si wafer. (**A**) AFM topography images and enlarged region of lymphocyte nucleus on undoped polished Si wafer. (**B**) Spectra acquired from points denoted by blue and red circles in A. (**C**) False colour images showing 2nd order phase shifts at 956, 1545 and 1845 cm^{-1}.

The nuclei did not lie as flat on this substrate as on AuSi; they remained slightly beaded up (Fig. 5A). Spectra from a thicker region (blue) and thinner region (red) were both dominated by protein Amide I and II bands (Fig. 5B). At the thinner location (blue spectrum), bands attributable to DNA are evident. The red spectrum in Fig. 5B includes bands at 1712, 1606, 1243, 1120-1050 and 960 cm^{-1} but these are much weaker than those in Fig. 3. That spectrum was acquired at a point where the 965 cm^{-1} band was close to maximum (Fig. 5C, top). The Amide I band seems to be strongest in the thick region (Fig. 5C, middle) but much of this is an artefact of sample thickness, since the increasing shift with increasing thickness increases persists even on the undoped Si wafer for thicknesses greater than 300 nm (Fig. 5C, bottom).

The DNA-poor circular regions are often located toward the periphery of the diseased nuclei.[1] Our preparation method of cytoplasmic strip followed by cytofuge deposition delivers bare nuclei of generally appropriate thickness. We conclude that this preparation along with the AuSi substrate is to be preferred, as it allows us to exploit tip-substrate coupling and obtain maximum signal from regions of critical interest.

Variations in spectra obtained with NFIR.

Many sSNOM near-field IR spectra were recorded from four whole lymphocytes and six stripped nuclei; for the latter, about 20 spots were sampled per nucleus, mainly at the target periphery. With optimization of the sample preparation methods, the quality of the spectra improved. Representative spectra of the 5 stripped nuclei for which data have been collected illustrate the frequently observed variations (Fig. 6).

Spectra from the same location in this nucleus were acquired at ALS, BL 5.4, with synchrotron illumination, and at Neaspec GmbH, with mid-IR lasers. The latter, shown in Fig. 3, with band assignments, are included here for comparison (Fig. 6 A, B). The red spectra (Fig. 6 A, C) are taken from the nuclear pore region; the blue spectra from chromatin-rich region (Fig. 6 B, D). Importantly, both experiments yielded the same results, demonstrating an excellent correspondence between spectra obtained with the mid-IR lasers and with synchrotron illumination, though the latter are noisier. The DNA band at 1710 cm^{-1} is also detectable in a suspected nuclear pore region of another cell (Fig. 6 E) but not at a denser location (Fig. 6 F), just as for the first nucleus. Pairs of spectra from two other nuclei (Fig. 6, G, H and I, J) were acquired in regions where thickness was 50-80 nm, using the Neaspec instrument at BL 2.4, ALS. While the 1710 cm^{-1} band was not resolved any of these spectra, the broad band around 960 cm^{-1} is quite clear. A strong band in this region is associated with DNA, but could have contributions from non-DNA phosphate.[25] These are the first such results and much more data must be collected to establish the variety of signatures in a statistically meaningful way. These first results show the enormous potential of the approach.

Fig. 6 Near-field infrared spectra acquired from stripped nuclei of several NL. (**A, B**) Spectra as in Fig. 3, cell 1, recorded with mid-IR lasers, Neaspec, GmbH; (**C, D**) SINS spectra from similar locations in the same cell, BL 5.4, ALS. Spectra from three other cells recorded with the Neaspec instrument at BL 2.4, ALS: (**E**, **F**) cell 2; (**G, H**) cell 3; (**I**, **J**) cell 4. A dip at 1265 owing to PDMS is visible in A, B, D and E.

Conclusions

The spatial resolution of superresolution fluorescence is a close match with that achievable with sSNOM type near-field infrared spectroscopy. We have developed a satisfactory method for preparing normal whole lymphocytes and stripped nuclei for near-field IR imaging at 30 nm voxel resolution (x,y defined by AFM tip, z defined by thickness. The NFIR spectra of points within stripped nuclei showed characteristic absorbances from protein, single and double stranded DNA, as well as hydrocarbon, ribose and phosphate signatures. NFIR images of bare nuclei at select wavelengths showed differences in distribution ascribable to nuclear pores and chromosome territories of the interphase nucleus. Comparison of sSNOM NFIR spectroscopy of cells mounted onto gold-coated wafers and onto undoped silicon wafers revealed an advantage for the former, believed to be due to enhancement at thinner regions (<30nm) due to tip-substrate dipole coupling. The combination of super resolution fluorescence imaging with near-field infrared spectroscopy and spectrochemical imaging allows unprecedented insight into the nanoscale architecture in normal lymphocyte nuclei. We anticipate that it will be similarly effective in diseased cells.

Conflicts of interest

SM is a Director and Chair of the Clinical and Scientific Advisory Board of 3D Signatures Inc. There are no other potential conflicts to declare.

Acknowledgements

The authors are grateful to Dr. Hans Bechtel (ALS, LBNL, Berkeley) for assistance in the collection of near-field IR data and images; to Dr. Christiaan H. Righolt (Vaccine and Drug

Evaluation Centre, Department of Community Health Sciences, The University of Manitoba) for conducting the original SRF experiments; and to Mr. Benoit Girouard (Department of Chemistry, The University of Manitoba) for assistance in creating the final figures. This research used resources of the Advanced Light Source, which is a DOE Office of Science User Facility under contract no. DE-AC02-05CH11231. The authors acknowledge funding from the Natural Sciences and Engineering Research Council (NSERC) of Canada (KMG), CancerCare Manitoba (761036238) and the Canadian Institutes of Health Research (123379) (SM). GCA is grateful to the University of Manitoba for a UofM Graduate Fellowship and a Graduate Enhancement of Tri-council Stipend Award; FC is grateful to the Regione Autonoma della Sardegna for fellowship funding.

References

1 C. H. Righolt, A. Guffei, H. Knecht, I. T. Young, S. Stallinga, L. J. van Vliet and S. Mai, *J Cell Biochem*., 2014, **115**, 1441-1448.
2 C. H. Righolt, H. Knecht, S. Mai, *J. Cell Biochem*. 2016, 117, 1633-1637.
3 C. Sathitruangsak, C. H. Righolt, L. Klewes, P. Tammur, T. Ilus, A. Tamm, M. Punab, A. Olujohungbe and S. Mai, *J. Cell Biochem*., 2015, 116, 704–710.
4 C. Sathitruangsak, C. H. Righolt, L. Klewes, D. Tung Chang, R. Kotb and S. Mai, *Int. J. Cancer*, 2017, **140**, 400-410.
5 A. Garcia, D. Huang, A. Righolt, C. Righolt, M. C. Kalaw, S. Mathur, E. McAvoy, J. Anderson, A. Luedke, J. Itorralba and S. Mai, *J Cell Physiol*., 2017, **232**, 2387-2395.
6 P. R. Griffiths and J. A. De Haseth, *Fourier Transform Infrared Spectrometry*, 2nd ed. John Wiley & Sons, 2007.
7 R. Hillenbrand, B. Knoll and F. Keilmann, *J. Microsc.*, 2001, **202**, 77-83
8 F. Keilmann and R. Hillenbrand, *Philos. Trans. Royal Soc. A*, 2004, **362**, 787-806.
9 I. Amenabar, S. Poly, W. Nuansing, E. H. Hubrich, A. A. Govyadinov, F. Huth, R. Krutokhvostov, L. Zhang, M. Knez, J. Heberle, A. M. Bittner, and R. Hillenbrand, *Nat. Commun*., 2013, **4**, 1-9.
10 H. A. Bechtel, E. A. Muller, R. L. Olmon, M. C. Martin and M. B. Raschke, *Proc. Natl. Acad. Sci. U.S.A*, 2014,
11 S. Mastel, A. A. Govyadinov, T. V. de Oliveira, I. Amenabar and R. Hillenbrand, *Appl. Phys. Lett*. 2015, **106**, 023113.
12 R. Wiens, C. R. Findlay, S. G. Baldwin, L. Kreplak, J. M. Lee, S. P. Veres and K. M. Gough, *Faraday Discuss.*, **187**, 555-573.
13 S. F. Louis, B. J. Vermolen, Y. Garini, I. T. Young, A. Guffei, Z. Lichtensztejn, F. Kuttler, T. C. Y. Chuang, S. Moshir, V. Mougey, A. Y. C. Chuang, P. Donald Kerr, T. Fest, P. Boukamp and S. Mai, *Proc. Natl. Acad. Sci. USA*, 2005, **102**, 9613-9618.
14 B. J. Vermolen, Y. Garini, S. Mai, V. Mougey, T. Fest, T. C.-Y. Chuang, A. Y.-C. Chuang, L. Wark and I. T. Young, *Cytometry A.,* 2005, **67**, 144-150.
15 R. Sarkar, A. Guffei, B.J. Vermolen, Y. Garini and S. Mai, *Cytometry A*., 2007, **71**, 386-92.
16 C. H. Righolt, V. Raz, B. J. Vermolen, R. W. Dirks, H. J. Tanke and I. T. Young, *Int J Mol Imaging*, 2011, **2011**, 723283.
17 S. Mathur, A. Glogowska, E. McAvoy, C. Righolt, J. Rutherford, C. Willing, U. Banik, M. Ruthirakuhan, S. Mai and A. Garcia, *J. Alz. Dis*., 2014, **39**, 35-48.
18 A. Garcia, S. Mathur, M. C. Kalaw, E. McAvoy, J. Anderson, A. Luedke, J. Itorralba and S. Mai, *J Alz. Dis*., 2017, **58**, 139-145.
19 A.-K. Schmälter, C. H. Righolt, A. Kuzyk and S. Mai, *Transl Oncol*., 2015, **8**, 417–423.
20 H. Knecht, N. Kongruttanachok, B. Sawan, J. Brossard, S. Prévost, E. Turcotte, Z. Lichtensztejn, D. Lichtensztejn and S. Mai, *Transl Oncol*., 2012, **5**, 269-277.
21 M. Gadji, A. J. Adebayo Awe, P. Rodrigues, R. Kumar, D.S. Houston, L. Klewes, T.N. Dièye, E.M. Rego, R.F. Passetto, F.M. de Oliveira and S. Mai, *Clin Cancer Res.,* 2012, **18**, 3293-3304.
22 Kuzyk, J. Gartner and S. Mai, *Transl Oncol*., 2016, **9**, 348-356.
23 P. Bassan, A. Sachdeva, A. Kohler, C. Hughes, A. Henderson, J. Boyle, J. H. Shanks, M. Brown, N. W. Clarke, and P. Gardner, *Analyst*, 2012, **137**, 1370-1377.
24 T. G. Mayerhöfer, and J. Popp, *Spectrochim. Acta A*, 2018, **191**, 283-289.
25 B. R. Wood, *Chem. Soc. Rev*, 2016, **45**, 1980-1998.
26 D. Cai, A. Neyer, R. Kuckuk and H. M. Heise, *J. Mol. Struct*, 2010,**976**, 274-281.

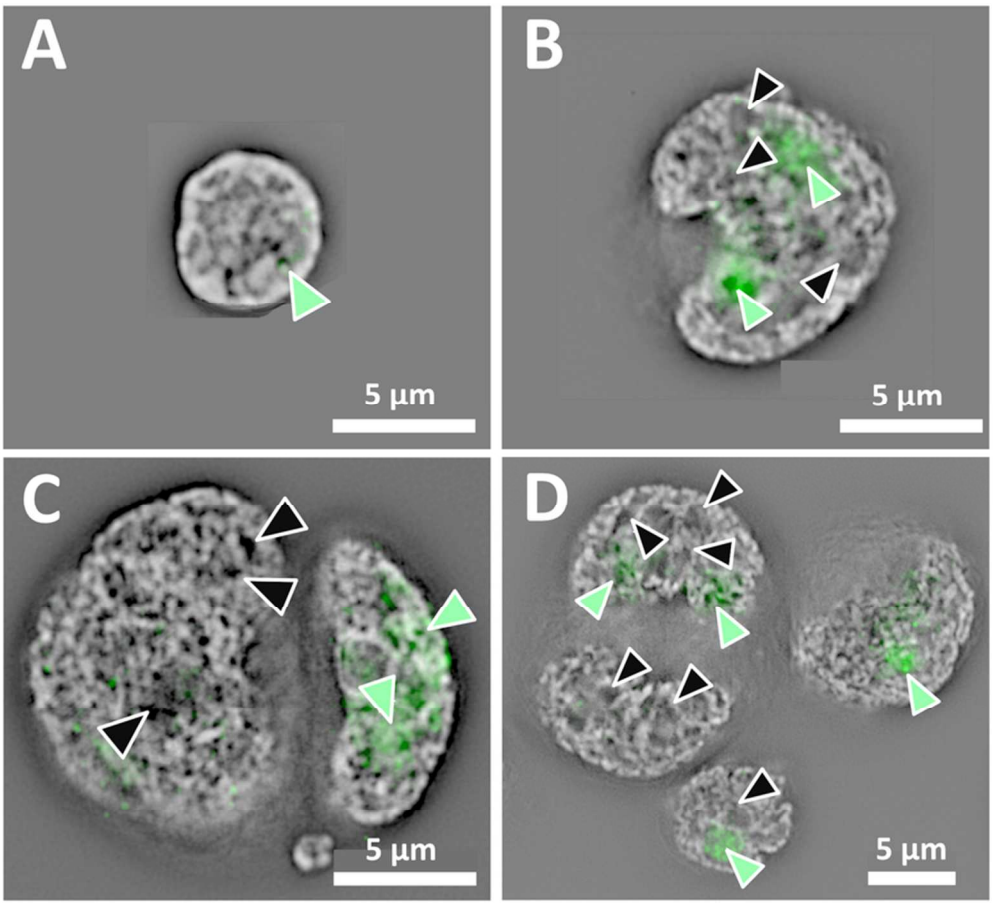

75x69mm (300 x 300 DPI)

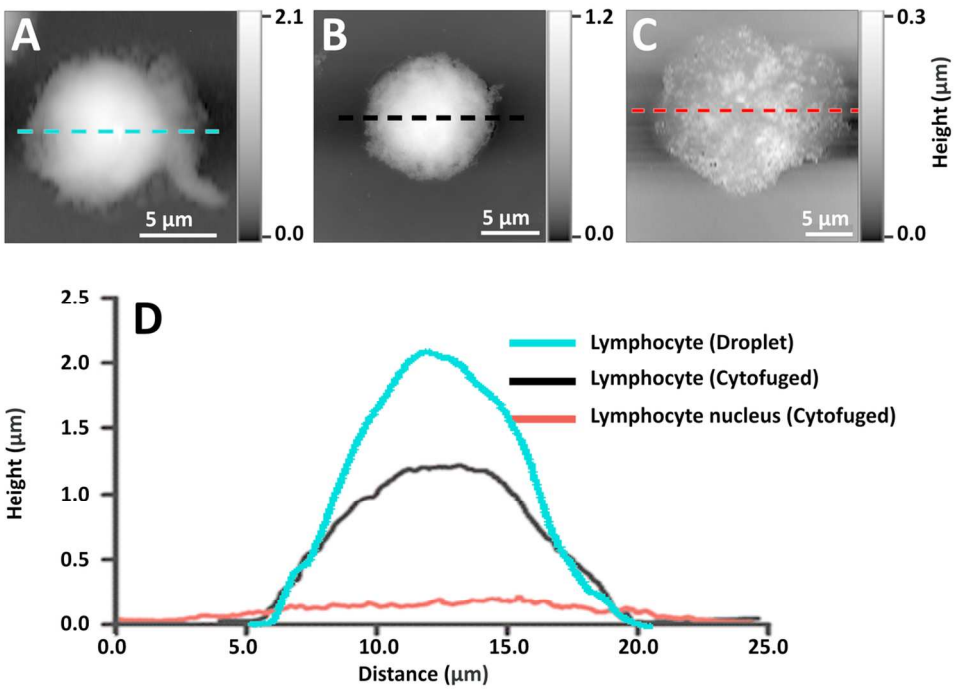

119x83mm (300 x 300 DPI)

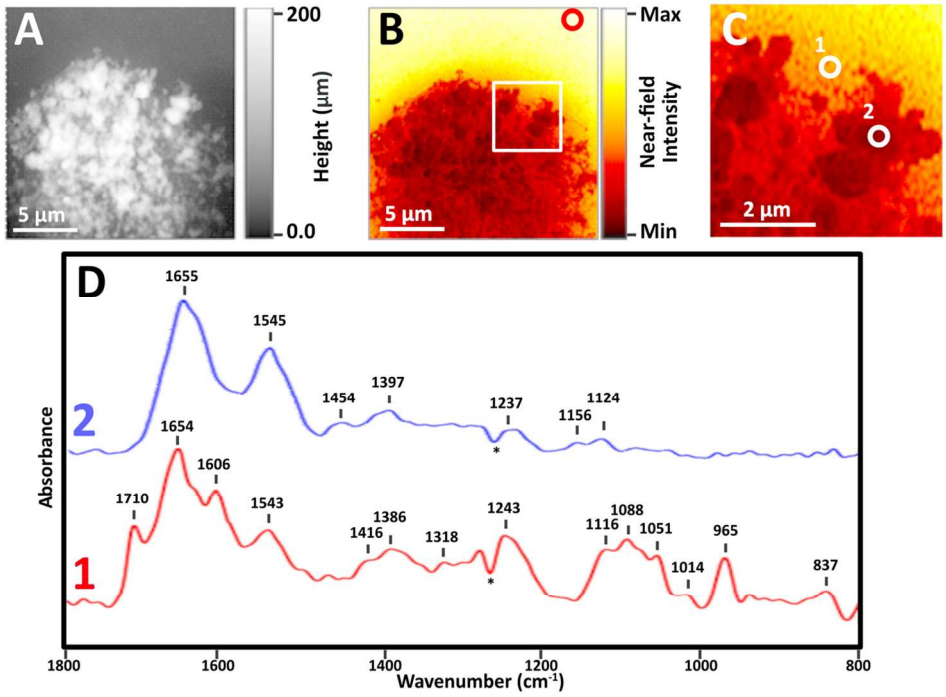

118x82mm (300 x 300 DPI)

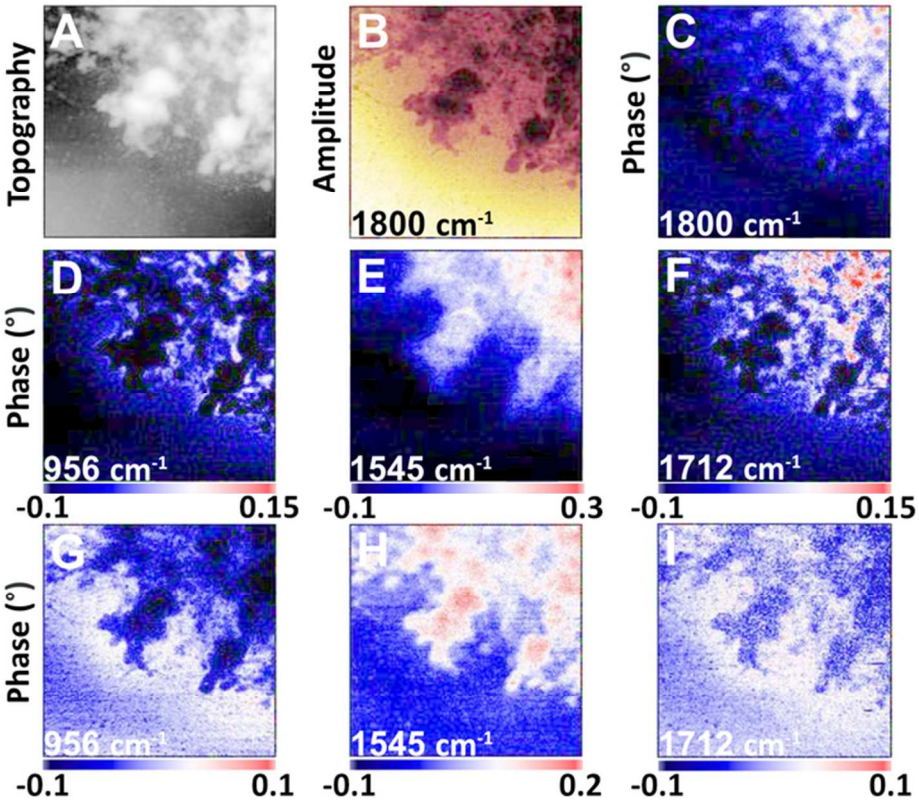

66x54mm (300 x 300 DPI)

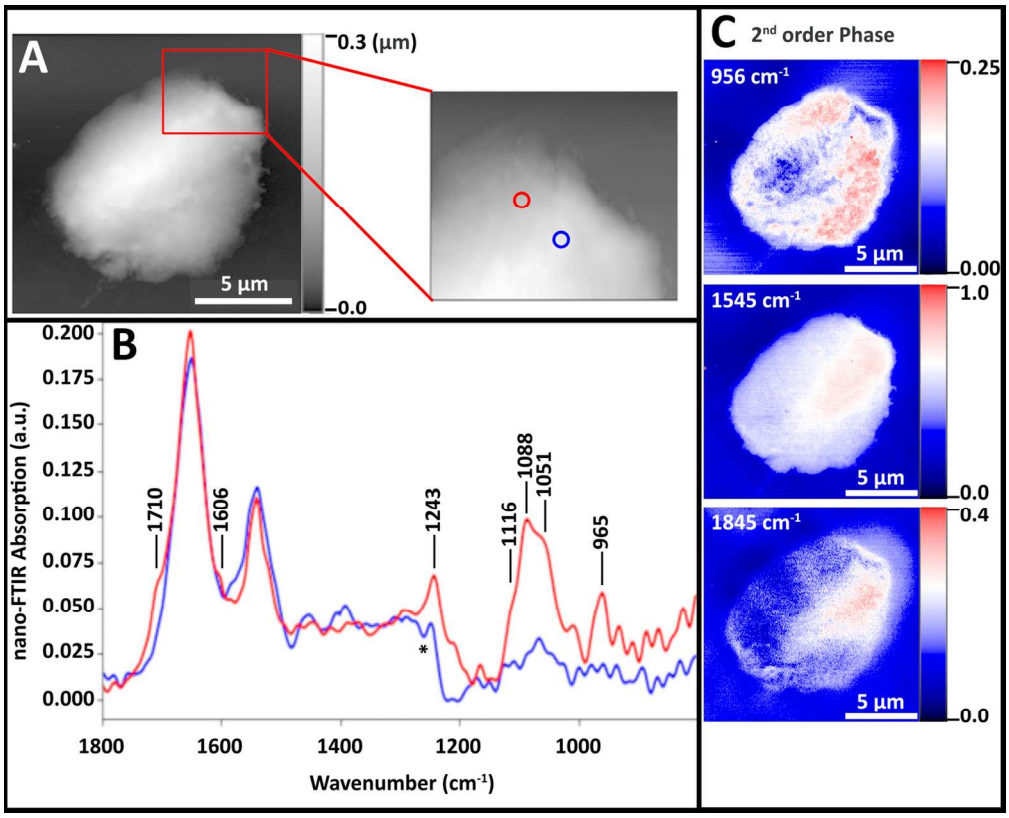

137x111mm (300 x 300 DPI)

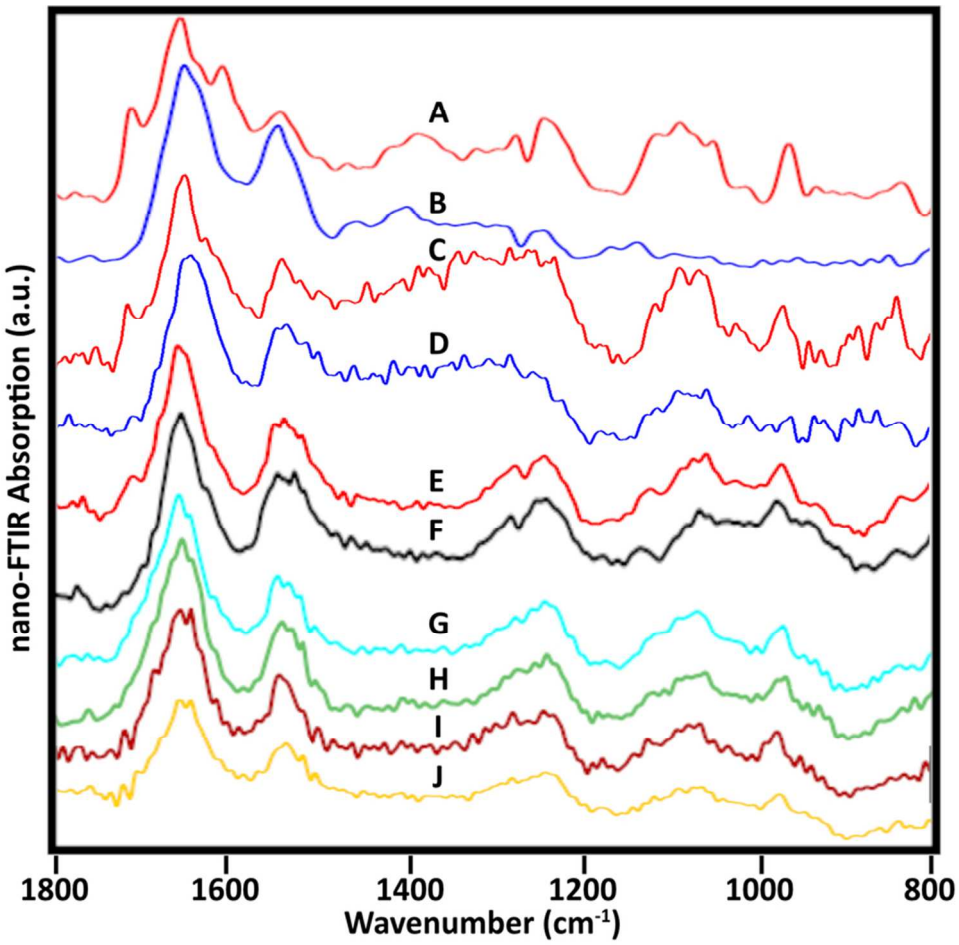

77x73mm (300 x 300 DPI)

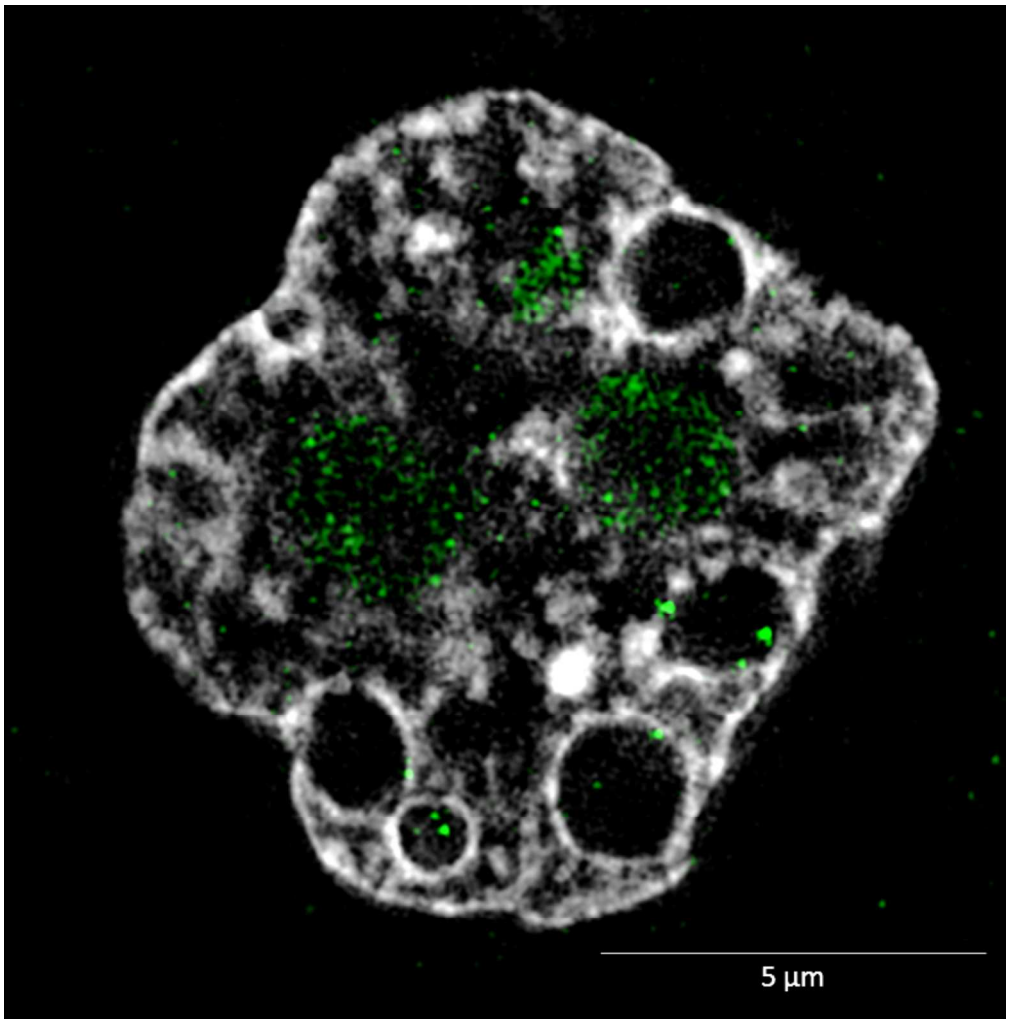
5 µm

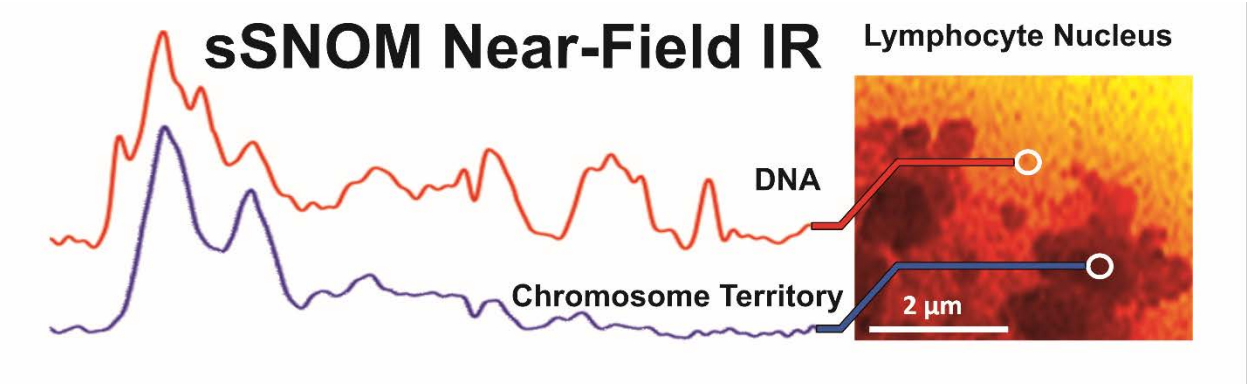

First Near-Field Infrared spectroscopy and imaging of lymphocyte nucleus at 30nm spatial resolution reveals spectrochemically distinct regions in nuclear organization.